Proceedings of:
ASME TURBO EXPO 2006
May 8-11, 2006, Barcelona, Spain

"DRAFT" **GT2006-90561**

An Experimental Investigation of Secondary Flows and Loss Development Downstream of a Highly Loaded Low Pressure Turbine Outlet Guide Vane Cascade

Johan Hjärne
Thermo and Fluid Dynamics
Chalmers University of Technology
412 96 Gothenburg, Sweden
johan.hjarne@chalmers.se

Régis Houtermans
Von Kárman Institute for Fluid Dynamics
Turbomachinery department
1640 Rhode-St-Genèse, Belgium
houterma@vki.ac.be

Valery Chernoray
Thermo and Fluid Dynamics
Chalmers University of Technology
412 96 Gothenburg, Sweden
valery@chalmers.se

Jonas Larsson
Department of Aero and Thermo Dynamics
Volvo Aero Corporation
461 81 Trollhättan, Sweden
jonas.larsson@volvo.com

Lennart Löfdahl
Thermo and Fluid Dynamics
Chalmers University of Technology
412 96 Gothenburg, Sweden
lennart.lofdahl@chalmers.se

ABSTRACT

This paper presents a detailed experimental investigation of the evolution of secondary flow field characteristics and losses at several measurement planes downstream of a highly loaded low pressure turbine/outlet guide vane (LPT/OGV). The experiments were conducted in a linear cascade at Chalmers in Sweden.
Several upstream realistic incidences and turbulence intensities have been investigated for one Reynolds number. Downstream characteristics have been measured by means of a 5-hole pneumatic probe. This allows for the determination of the mean vortical structures, their development and their interactions. The trailing edge vortices, the two branches of the passage vortex and the corner vortex are clearly visible close to the blade trailing edge. Their intensity is shown to be strongly dependent on the inlet flow angle. The turbulence level seems to play a role on the mixing inside and between the structures. The measurements also show the dependence of the losses along the blade span on the development of the vortices.

1 INTRODUCTION

Cost and weight requirements on modern jet engines often lead to more highly loaded turbines with fewer stages. In un-geared two and three shaft engines, this gives higher swirl angles into the LPT/OGV. This makes the aerodynamic design of the OGV more difficult. Structural requirements also often lead to non-cylindrical shrouds with complex 3D polygonal shapes and sunken engine-mounts with bumps protruding into the gas channel. This has sparked a renewed interest in design methods and validation cases for 3D OGV flows. Secondary flows intensities are directly related to the loading and therefore to the passage turning. This latest being more important for turbine than for compressors cascades, most of the literature, if not all, is dedicated to turbine flows. In absence of a suction side separation, the physics of the secondary flows is expected to be relatively the same for both types of cascades.

A good literature survey for secondary flows in turbine cascades was written by Sieverding [1] in 1985. The endwall inlet boundary layer impinges on the blade leading edge and rolls up to form a horseshoe vortex with two branches on each side. The pressure side legs, under the influence of the transverse pressure gradient, are directed towards the suction side of the neighboring blade where it interacts with the suction side legs of the horseshoe vortex. The pressure side legs form with the cross flow the passage vortex. The suction side leg lifts up away from the endwall and orbits around the passage vortex as it is convected downstream. Depending on the interaction strength, a corner vortex develops along the suction side corner. A new highly skewed endwall boundary layer forms and develops downstream the second pressure side leg separation line. The downstream loss distribution is mainly a function of

the loading, the inlet boundary layer characteristics and the downstream distance. In the conclusion, the author insisted on the fact that, beside an increased knowledge of the separation line patterns, more experiments were needed to determine each factor influence.

Another factor of interest, the turbulence intensity, has been investigated by Gregory-Smith and Cleak [2]. They measured the secondary turbulent kinetic energy development through the cascade under low and high freestream turbulence intensities. Their measurements are of great interest not only for the flowfield determination but also for CFD modeling. Moreover, they pointed out that the inlet turbulence intensity has no major influence on the mean flow development and that it has a limited influence on the gradient of loss evolution through the cascade, the secondary turbulent kinetic energy reaching a maximum close to the blade trailing edge. For a given loading, the loss level seemed to be directly linked to the inlet boundary layer integral properties. Their conclusion about the loss evolution was confirmed by Sharma and Buttler [3]. For straight cascades with high aspect ratio (no interactions between opposite endwalls secondary flows), they provided a correlation based on inlet boundary layer features and passage turning angle to estimate the secondary flows extension at trailing edge suction surface. They finally came out with a correlation for the total losses.

The secondary flow pattern has been investigated trough visualizations by Wang et al. [4] and through accurate heat transfer measurements by Goldstein and Spores [5]. They confirm Sieverding's review and they add some important features about the development of the secondary flowfield. A horseshoe corner vortex is present beside the usual horseshoe vortex at leading edge. The suction side leading edge corner vortex is stretched by the acceleration and is lifted up along the suction side close to the position were the passage vortex interacts with the suction side horseshoe vortex. This leading edge corner vortex remains along the blade surface further downstream where the passage vortex separates from the suction side. Visualizations of Kawaï et al. [6] show that the pressure side leading edge corner vortex most probably forms the pressure side corner vortex.

The aim of this paper is to present the downstream interaction between the passage secondary flows and the trailing edge vortices as well as the performance evolution with downstream distance of a typical modern highly loaded LPT/OGV. This will be done for a fixed inlet boundary layer height with varying inlet turbulence intensity and flow incidence.

NOMENCLATURE

C	Blade chord [m]
Cp	Pressure coefficient
P_s	Static pressure [Pa]
P_{tot}	Total pressure above atmospheric pressure [Pa]
P_{dyn}	Dynamic pressure based on the inlet velocity [Pa]
P_{fs}	Total pressure outside the down stream wakes [Pa]
Re_c	Reynolds number = $U_1 C/\nu$
Tu	Turbulence intensity [%]
x	x-coordinate
y	y-coordinate
z	z-coordinate

Greek Symbols

δ	Boundary-layer height [mm]
ξ	Total pressure losses = $(P_{fs}-P_{tot})/P_{dyn,1}$

Acronyms

LPT	Low pressure turbine
OGV	Outlet guide vane

2 EXPERIMENTAL SETUP

The linear cascade used for these measurements is an open circuit blower type. A 30kW fan is used to drive the flow through a diffuser, a flow straightener (consisting of a honeycomb and three screens with different porosity). The flow is accelerated in a 5:1 contraction before it enters the test section. The test section is built up of four parallel discs, two on each side, where the inner discs constitutes side walls for the 7 OGV which forms the cascade. The gap between the inner and outer discs is used for sucking out the boundary layers developed in the upstream sections. There is one separate suction system on each side driven by two 7.5kW motors. The two suction systems can thus be adjusted independently in such a way that the wall static pressure on both sides of the test section is equal. This has to be done for each incidence angle that can range continuously from 0 to 52 degrees by rotation of the outer side walls. A more detailed description of the test-facility has been earlier given by Hjarne et al. [7,8]

The grid used for generation of free stream turbulence consisted of 5mm bars with a mesh size of 25mm giving a solidity of 0.31. It was placed 450mm upstream of the cascade and parallel to the leading edge plane, see Fig. 1. Besides increasing the turbulence intensity from 0.5% to 5%, the parallel grid has two effects. The positive one is that the inlet turbulence intensity is uniform in front of the cascade. But, as it deflects the flow, the outer side wall inclination had to be adapted so that the inlet incidence remained unchanged.

This OGV was designed to create experimental validation cases for numerical simulations. It is a 2D geometry profile which is extended in the span direction (z-direction). The on-design requirements for this vane is to turn an incoming flow field with an incidence of 30 degrees to an axial outflow with as low total pressure loss as possible. A typical off design requirement on LPT/OGV's is that they should not separate completely in the range of ± 10 degrees incidence. The cascade geometry data are given in table 1.

The periodicity has been checked and is illustrated in Fig. 2 and Fig. 3. The first one shows the static pressure distribution around the three mid vanes. The variation from one vane to another is small for both the suction side and the pressure side. The second gives the total pressure distribution at midspan 0.8 chords downstream the trailing edge plane.

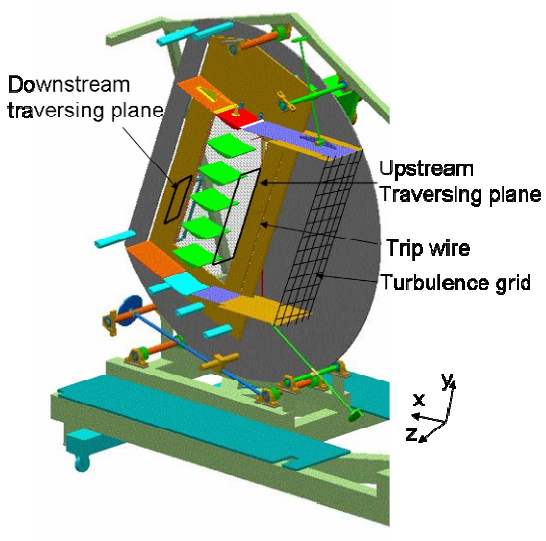

Figure 1 Picture of the experimental set up.

Table 1 Cascade geometry data

Number of vanes	7
Chord length (m)	0.22
Pitch to chord ratio	0.91
Aspect ratio (Span to Chord ratio)	0.91
Inlet Reynolds number	280000
Incidence angles (°)	20,30,40
Turbulence intensity (%)	0.5 or 5
Incoming boundary layer height (mm)	7.15 - 9.6

Instrumentation

Two traversing systems have been used to measure the flow field both upstream and downstream. The movements in the (y, z) plane is controlled by stepper motors with a minimum accuracy of 12.5µm. The five hole pressure probes used for the upstream and downstream traverses have been manufactured at Chalmers and was calibrated between –20 to 20 degrees for both pitch and yaw angles.

The inlet measurements were conducted 1.3*C upstream of the cascade with square grid cells of 20mm in size. The typical total pressure variation was below 2% of the dynamic head. The upstream traversing system has also been used to measure the incoming boundary layer height along the side walls. In order to a reach boundary layer height similar to what is present in a real engine, the boundary layer were tripped with a 1.5 mm wire placed 1.4*C in the flow direction in front of the blade leading edge plane.

The height of the fully developed turbulent boundary layer was 9.6mm and 7.15mm respectively with and without the turbulence grid inserted. They were measured 0.91*C in the flow direction upstream the leading edge plane. The downstream traversing system can be moved manually in the x direction with an accuracy of ± 0.0025*C. As the test rig has very good periodicity and symmetry, see Hjarne et al. [8], the outlet measurements were taken for half a span one pitch over

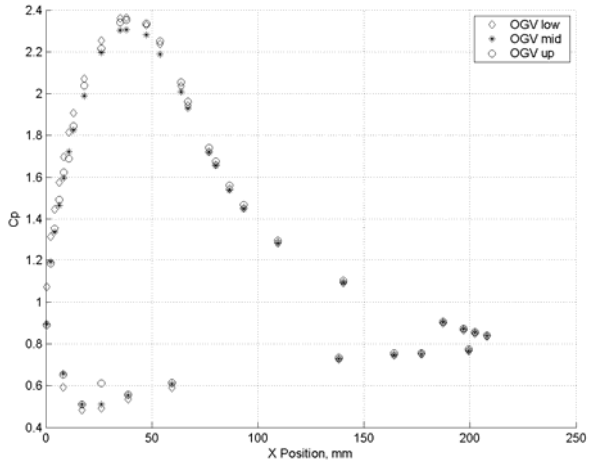

Figure 2 Cp distributions for the three mid OGV in the cascade.

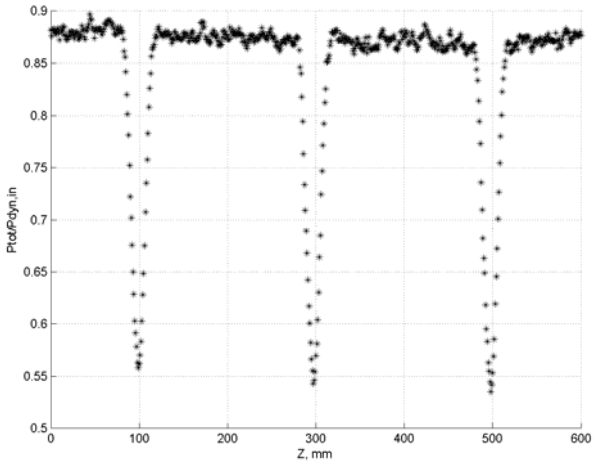

Figure 3 Downstream wakes of the total pressure normalized with inlet dynamic head.

the central blade at three different streamwise locations downstream of the trailing edge (0.25*C, 0.5*C and 0.8*C). A discretization of 2mm in each direction was used. To avoid wall proximity effect, as suggested in [9], the flow field was not measured at a distance lower than two times the probe head size from the endwall.

3 RESULTS AND DISCUSSION

Complete investigations of an OGV downstream passage have been made with a 5-hole pressure probe. A time mean value of the flow field variables can thus be deduced. Beside the losses and outlet flow angles, thanks to a high plane discretization, it was possible to compute the streamwise vorticity. Even if it allows for a better understanding of the development of the secondary flows than the distributed total pressure losses, the interpretation of the results requires caution. The reason is multiple. First, the probe has a finite head size with respect to the vorticity field. Then the probe calibration is normally dependent on the turbulence intensity and anisotropy. Gregory-

Smith and Cleak [2] have measured turbulence intensities up to 30 % in the loss core, which, from [9], can lead to an uncertainty on the measured pressure of 3%. Finally, pressure measurements do not resolve the time variation of the flow. These factors have an influence on the measured absolute value or on the point-to-point variation, but this should not affect a global interpretation. It also has to be noticed that the color scale used for plotting the results varies from for the different downstream positions. This has been done to account for the downstream diffusion and to keep the vorticity distribution as much visible as possible. For all the vorticity pictures, the pressure side points towards the top and the suction side towards the bottom (pitch = 0), the sidewall standing on the left.

20deg inlet flow angle

Streamwise vorticity for the lowest inlet flow angle are presented on Fig. 4-6 and Fig. 7-9 respectively with and without a turbulence grid. Closest to the blade trailing edge, on Fig. 4, the passage vortex is visible in red. Its extension is rather small and it is located very close to the endwall. The blue vertical area on the left represents the secondary flow in the endwall boundary layer, which thickness increases from pressure to suction side. No corner vortex appears. The low turning reduces the loading and also the interaction of the passage vortex with the cross flow in the end wall boundary layer. Sieverding [1] explained that for these conditions, the corner vortices may not be present. Another reason would be that the first measurement is too far away from the endwall to detect it. The last recognizable feature is the rectangular blue pattern present in the blade wake. It is attributed to the trailing edge vortex sheet which arises due to the spanwise change of the blade circulation.
The relative evolution of these vorticity fields is depicted in the two next figures. The passage vortex core seems to remain at the same position, even if its extension or its strength are respectively, gradually increasing and decreasing. The passage vortex also interacts with the growing endwall boundary layer, bringing some low momentum fluid to the main flow. The trailing edge vortex sheet is stretched into two parts. The main one concentrates in direction of the passage vortex, while the secondary forms closer to mid span. In absence of flow visualization, nothing can be stated for the formation of trailing edge vortices, but it seems that the trailing edge vortex sheet splits and roll up to form two distinct vortices. This trend will become clearer after the analysis of the low inlet turbulence intensity measurements.

The inlet boundary layer thickens with an increase of the turbulence intensity, the shape factor (displacement thickness/momentum thickness) being for both cases equal to 1.41. Surprisingly, the vorticity magnitude in the passage vortex core is in this case generally lower than for the low inlet turbulence. Considering the streamwise derivative negligible, the variation of the velocity with the distance normal to the wall is by definition the normal vorticity (y component). The velocity has been interpolated over a distance of 0.2 mm till the wall. The integral of the computed vorticity across the boundary layer is constant. The overall vorticity content is therefore equivalent. The main difference lies in the velocity gradient close to the wall. In this case, the low to high turbulence intensity ratio of the normal vorticity is shown to be approximately equal to the ratio of the boundary layer heights: 1.35. Praisner and Smith [10] have shown that the inlet boundary layer is forced to separate from the endwall as it approaches the leading edge. The vorticity is then redistributed into the different structures that compose the horseshoe vortex. It is thus supposed that the difference in the vorticity magnitude downstream is directly related to the vorticity concentration inside the inlet boundary layer, while, from Sharma and Butler [3], the inlet boundary layer thickness should have an influence on the secondary flows extension at the blade trailing edge.

The shearing action of the trailing edge vortex sheet deformation leads it to split into several small parts which probably roll up into vortices, see Fig. 7. It contrasts with the high inlet turbulence intensity case for which the turbulent Reynolds stresses most likely prevent the multi-part splitting. These vortices die out by the action of diffusion and dissipation. The passage vortex influence on the endwall boundary layer is also more significant. The amount of low momentum fluid extracted is rather important. As the trailing edge vortex does not anymore concentrate close to the passage vortex and because the strength of this latest is more important, it allows a stronger interaction. This observation could also show that the endwall boundary layer is somehow more laminar compared to the previous case. The newly forming boundary layer has a turbulent background that is lower. For the same downstream deceleration rate, this influences the shear layer transition process as well as the internal mixing.

30deg inlet flow angle, design point

The blade loading changes as the inlet flow angle increases to 30 degrees. The magnitude of the adverse pressure gradient on the blade rear suction side is enhanced and the transverse pressure gradient from pressure to suction side is increased. These combined effects influence the crossflow magnitude as well as the secondary flows strength, size and position. This situation is depicted in Fig. 10-12 for high inlet turbulence intensity.

The endwall boundary layer is slightly thicker than for the lowest inlet flow angle. The passage vortex is now located further from the endwall. This position change could be explained by two factors that are probably not independent. The first one is the strengthening and growing of the vortical structure. The second factor lies in the interaction between the passage vortex and the trailing edge vortex sheet. This latest still splits into two parts. A small one is close to midspan and the main part is now close to the wall on the other side of the passage vortex. The “S” shaped tails of the passage vortex and the main trailing edge vortex is a clue of their mutual interaction. Two explanations can be given for the existence of a light blue region underneath the passage vortex. Whether it is the suction side leg of the horseshoe vortex or it is a part of the trailing edge vortex sheet deformed by the action of the horseshoe vortex. Traveling downstream, the vortices move towards midspan.

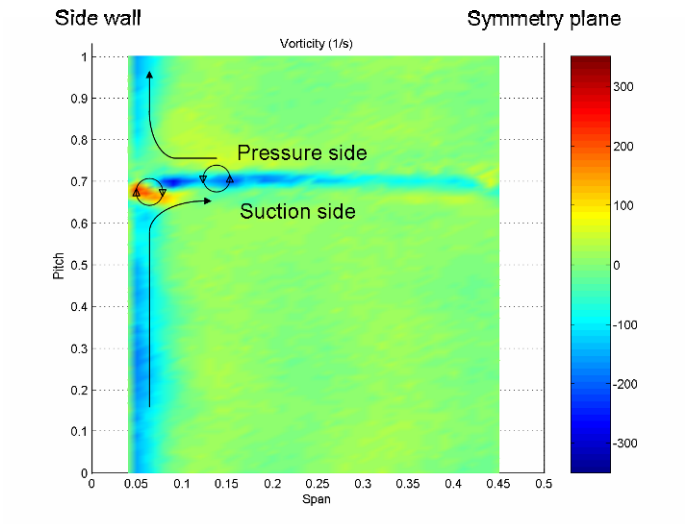

Figure 4 Vorticity 0.25*C downstream with Tu=5% and the inlet flow angle =20deg

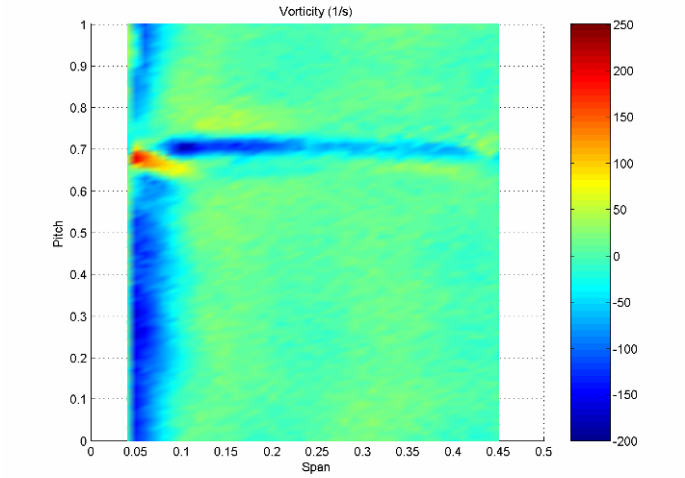

Figure 5 Vorticity 0.5*C downstream with Tu=5% and the inlet flow angle 20deg

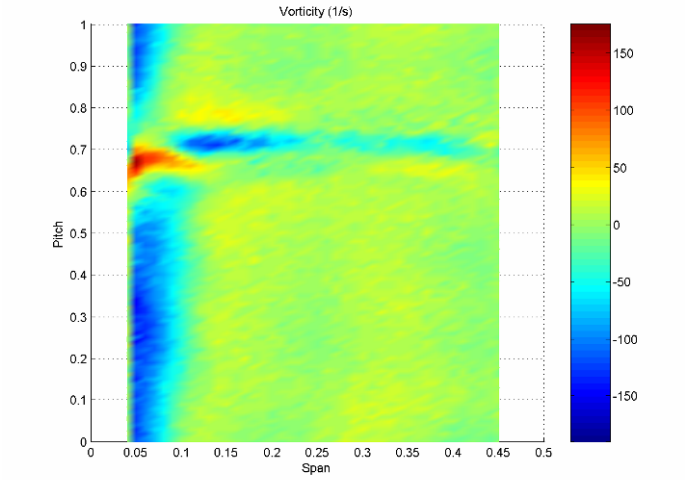

Figure 6 Vorticity 0.8*C downstream with Tu=5% and the inlet flow angle 20deg

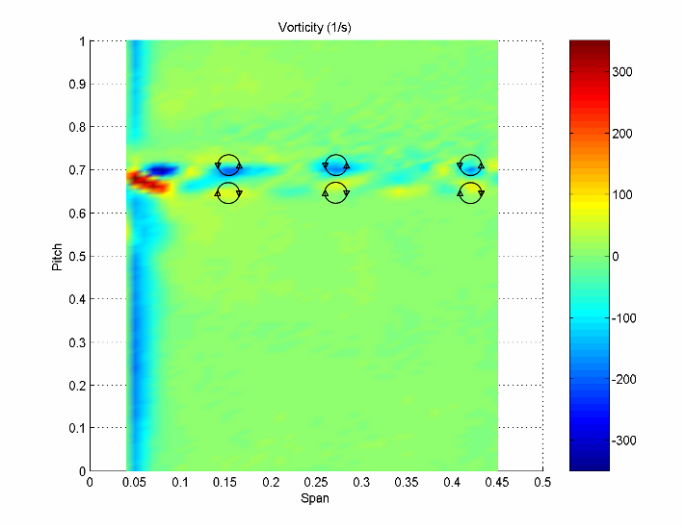

Figure 7 Vorticity 0.25*C downstream with Tu=0.5% and the inlet flow angle 20deg

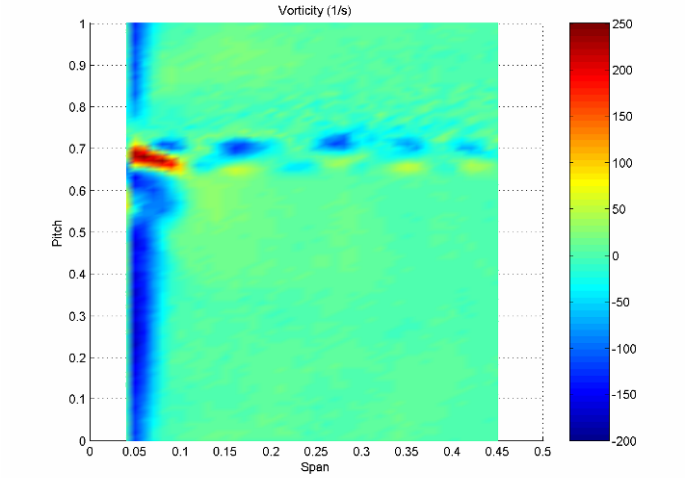

Figure 8 Vorticity 0.5*C downstream with Tu=0.5% and the inlet flow angle 20deg

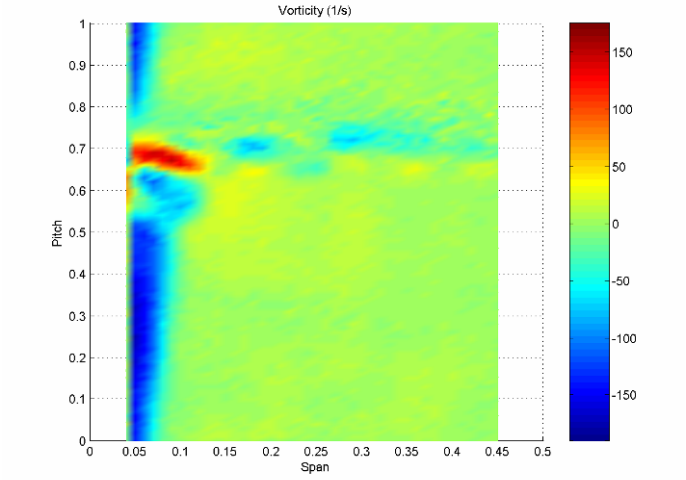

Figure 9 Vorticity 0.8*C downstream with Tu=0.5% and the inlet flow angle 20deg

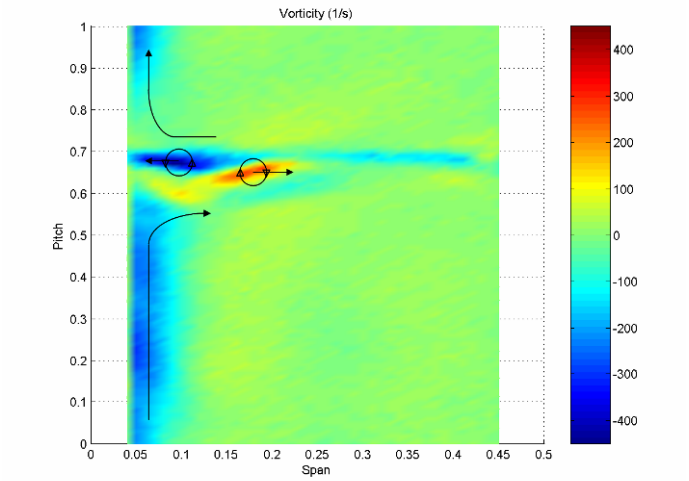

Figure 10 Vorticity 0.25*C downstream with Tu=5% and the inlet flow angle 30deg

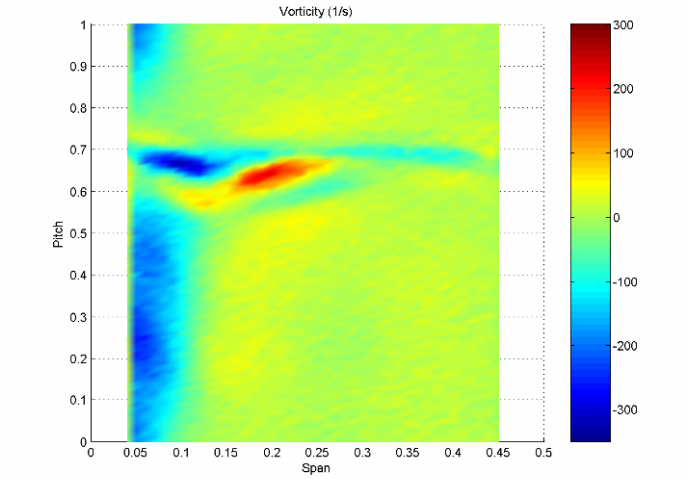

Figure 11 Vorticity 0.5*C downstream with Tu=5% and the inlet flow angle 30deg

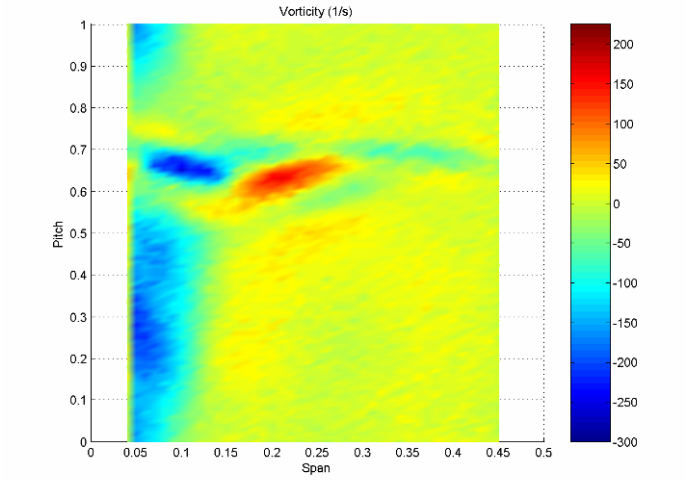

Figure 12 Vorticity 0.8*C downstream with Tu=5% and the inlet flow angle 30deg

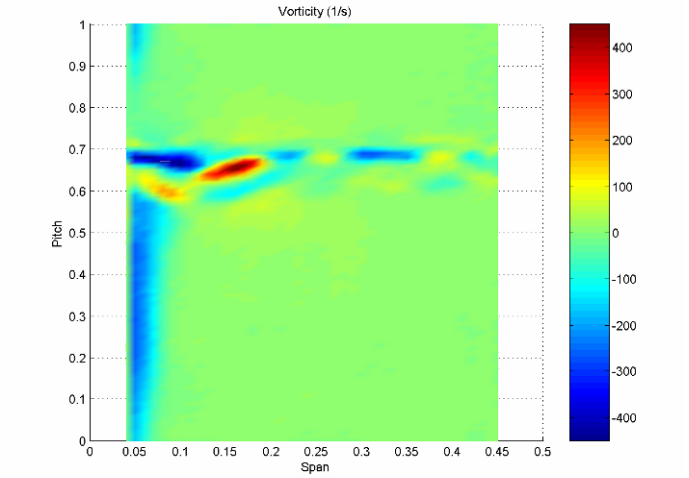

Figure 13 Vorticity 0.25*C downstream with Tu=0.5% and the inlet flow angle 30deg

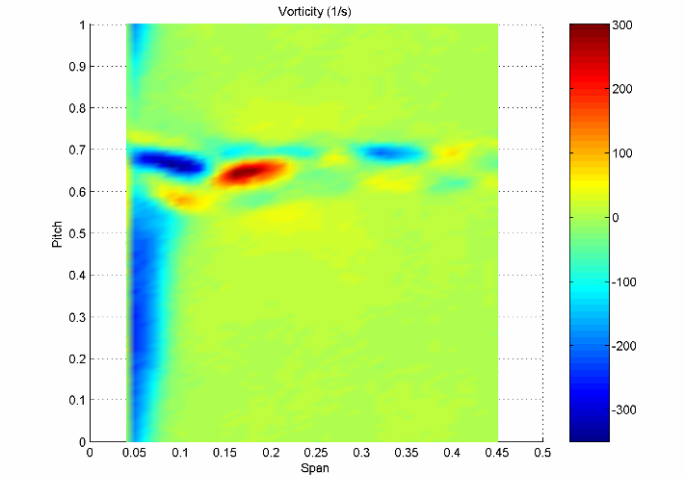

Figure 14 Vorticity 0.5*C downstream with Tu=0.5% and the inlet flow angle 30deg

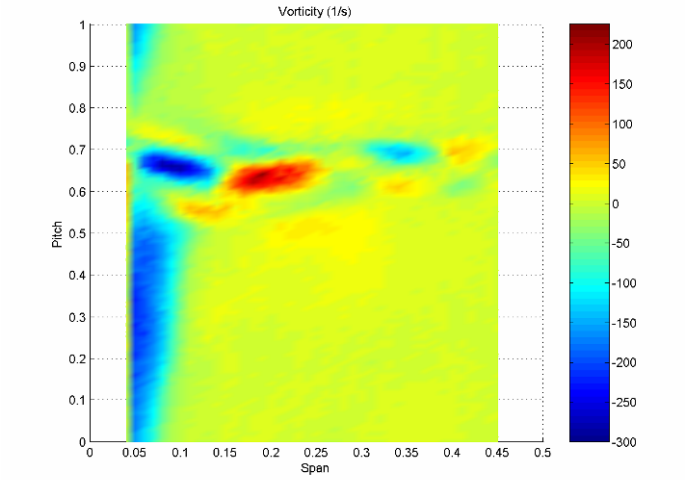

Figure 15 Vorticity 0.8*C downstream with Tu=0.5% and the inlet flow angle 30deg

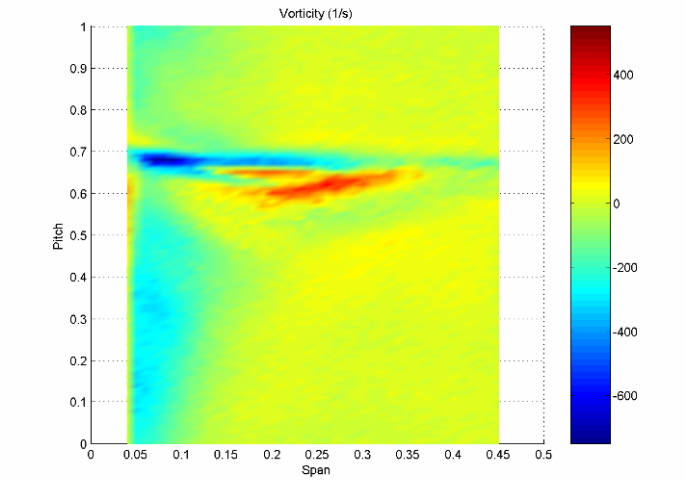

Figure 16 Vorticity 0.25*C downstream with Tu=5% and the inlet flow angle 40deg

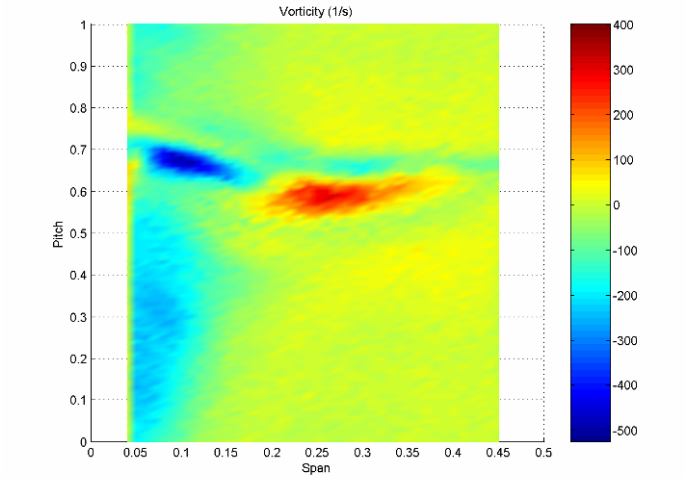

Figure 17 Vorticity 0.5*C downstream with Tu=5% and the inlet flow angle 40deg

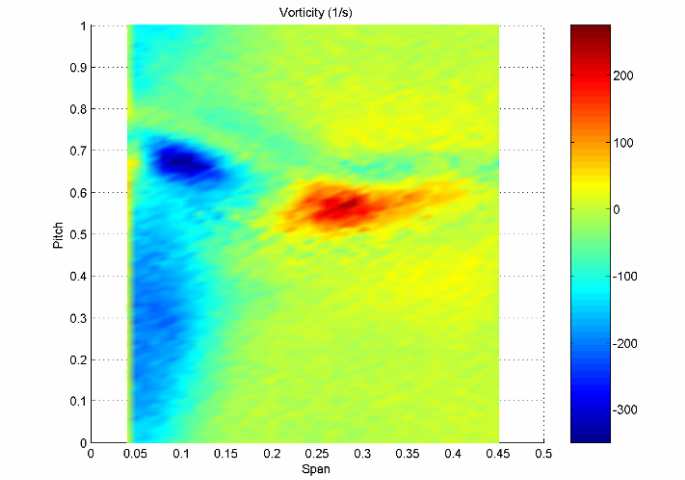

Figure 18 Vorticity 0.8*C downstream with Tu=5% and the inlet flow angle 40deg

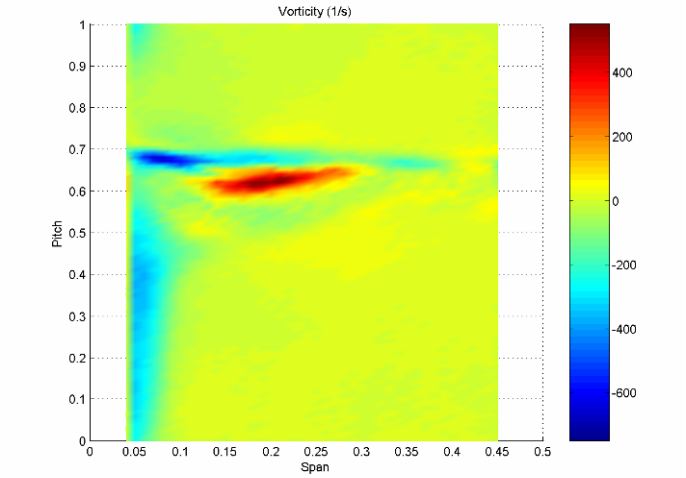

Figure 19 Vorticity 0.25*C downstream with Tu=0.5% and the inlet flow angle 40deg

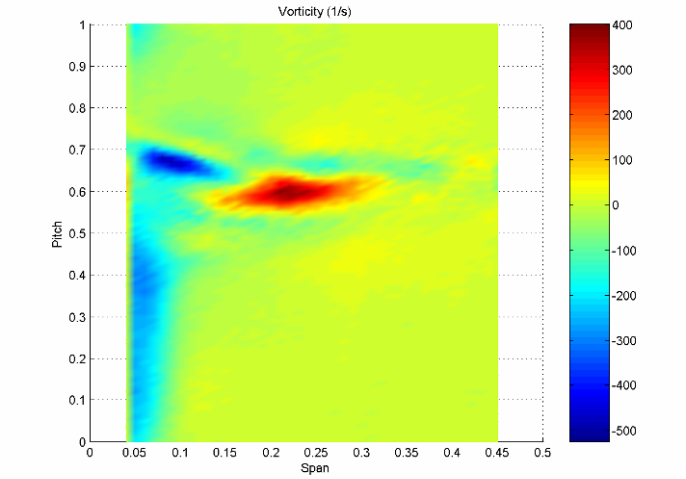

Figure 20 Vorticity 0.5*C downstream with Tu=0.5% and the inlet flow angle 40deg

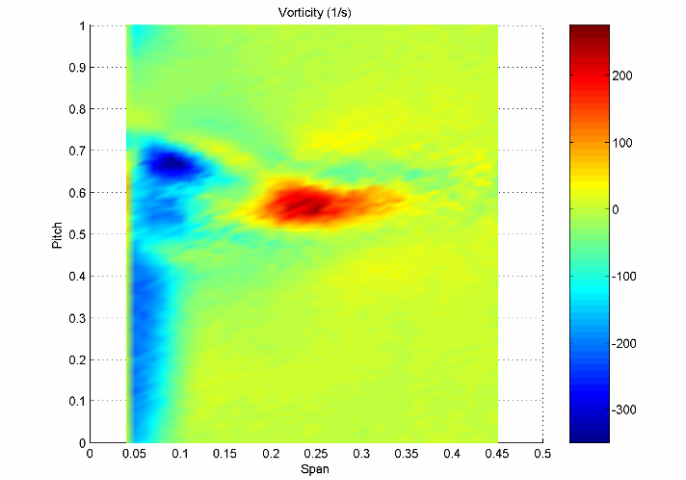

Figure 21 Vorticity 0.8*C downstream with Tu=0.5% and the inlet flow angle 20deg

Furthermore, their strength reduces and they grow in size by the action of the diffusion and dissipation processes.

The results for lower inlet turbulence intensity are represented on Fig. 13-15. As for the previous inlet flow angle, the endwall boundary appears to be thinner than with high inlet turbulence. The relative different properties of the passage vortex are linked to the features of the inlet boundary layer. On one hand, the higher vorticity content is directly related to the higher inlet boundary layer vorticity concentration. On the other hand, the smaller extension and the smaller endwall distance of the passage vortex are associated with the inlet boundary layer thickness. Again, the effect of the higher turbulence intensity is mainly to ensure an increased coherence of the vortical structures. The trailing edge vortex sheet is now split within three parts: one major close to the wall, a minor one that interacts with the passage vortex and dies out very fast and a last one close to midspan that rolls up and induces the formation of vorticity around it. The major trailing edge vortex has a more unilateral influence on the passage vortex. Only this latest tail is torn in "S" shape by shearing action.

40deg inlet flow angle

Figures 16-18 show the downstream streamwise vorticity development for high inlet turbulence intensity. A further increase of the loading let appearing the two main structures of the secondary flows: the trailing edge vortex sheet rolling up into a vortex and the passage vortex. It moves towards midspan as it is convected downstream. Their mutual interaction is reduced even if the passage vortex position still forces the trailing edge vortex to form close to the endwall. This low aspect ratio blade probably leads to the interaction at midspan of the two sidewalls passage vortices. The endwall boundary layer is again thicker. It now feeds in the trailing edge vortex. The bump in its vorticity distribution seems to show that low momentum fluid is attracted by the passage vortex. The lower turbulence intensity influence, given in Fig. 19-21, is now rather limited to the feeding process of the trailing edge vortex by the endwall boundary layer low momentum fluid. The inlet boundary layer thickness and vorticity concentration still modify the passage vortex size, position and strength.

4 LOSSES

The spanwise total pressure loss distributions for the different downstream positions are plotted in Fig 22-25. The losses are calculated as the mass averaged value of total pressure difference between inlet and outlet divided by the inlet dynamic head.

30 deg inlet flow angle and different downstream positions

The high inlet turbulence intensity case shown on Fig. 22 has several interesting characteristics. First, the midspan value of the losses does not vary with the downstream distance. It seems that no mixing but only dissipation takes place at this position. This suggests that the trailing edge vorticity sheet does not roll up close to midspan. Then, the minimum value of the losses is reached between the passage vortex and midspan. This is other evidence that the trailing edge vortex sheet is torn and that the vorticity concentrates in two different locations. Finally, the trailing edge vortex together with the boundary layer leads to an increased value of the losses close to the endwall. The passage vortex loss core induces a bump in the losses distribution around the 0.2 span locations. The variation in the loss shape is directly related to the mixing process for its downstream increasing value and to the secondary flows migration towards midspan for the bump displacement.

By comparison with the low inlet turbulence intensity case of Fig. 23, several differences can be found. Close to the endwall, the interaction between the main trailing edge vortex and the passage vortex induce a higher mixing and so a different downstream loss evolution. Towards midspan, the passage vortex loss bump is followed by a second one. This latest, linked to the trailing edge vorticity concentration, migrates and slightly increases as the flow is convected downstream. Finally, the level of the losses is higher in the passage vortex loss core as a result of the higher vorticity magnitude.

Inlet flow angle effect on downstream losses

Figures 24 and 25 show the losses for various inlet flow angles at the last downstream plane, respectively with and without turbulence grid. At high inlet turbulence, the change of pattern from 20 to 30 degrees is linked to the secondary flows evolution. The passage vortex and the trailing edge vortex flip over while the trailing edge vortex sheet is split in two parts. For an even higher turning, this sheet mainly concentrates into one single vortex close to the endwall. Moreover, both vortical structures are fed by the endwall low momentum fluid. The passage vortex increases in size and strength and moves to midspan where it could start interacting with the opposite one. It is also clear that changing the incidence to a positive one has a strong impact on the losses level.

Figure 25 for the low turbulence intensity depicts relatively the same evolution. One major difference for the lowest inlet flow angle is the losses plateau encountered over a wide part of the span. It contrasts a lot with its high turbulence evolution. This difference is thought to be related to the splitting of the trailing edge vortex sheet into several smaller parts. The level of the losses is generally higher but for the 40° inlet flow angle. By comparison of Fig. 18 and Fig. 21, this difference has to be linked to the interaction processes between the endwall boundary layer and the secondary flows. The passage vortex is also further from midspan and cannot yet interact with the one from the other sidewall.

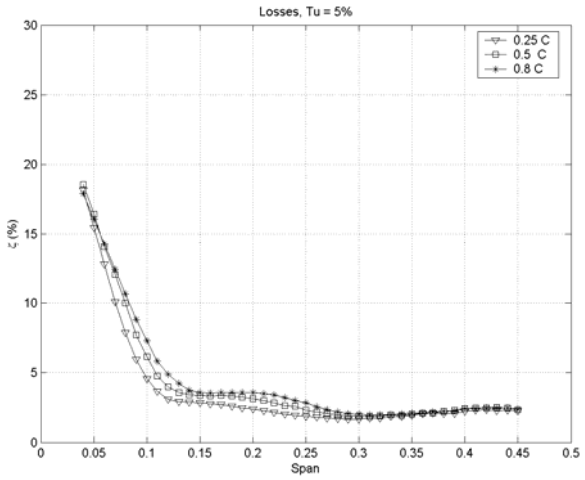

Figure 22 Losses for an inlet flow angle of 30 deg and Tu=5% at varying positions downstream

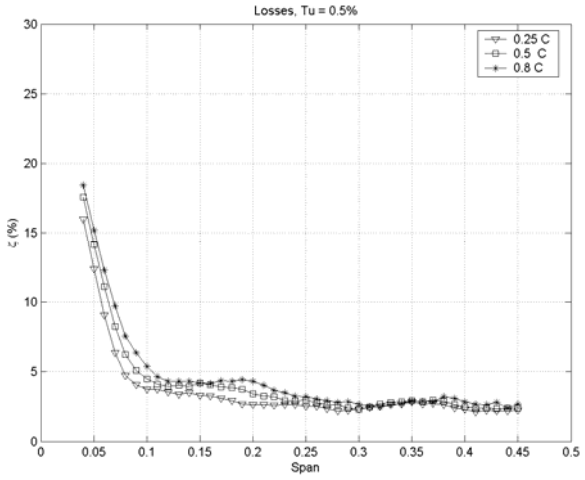

Figure 23 Losses for an inlet flow angle of 30 deg and Tu=0.5% at varying positions downstream

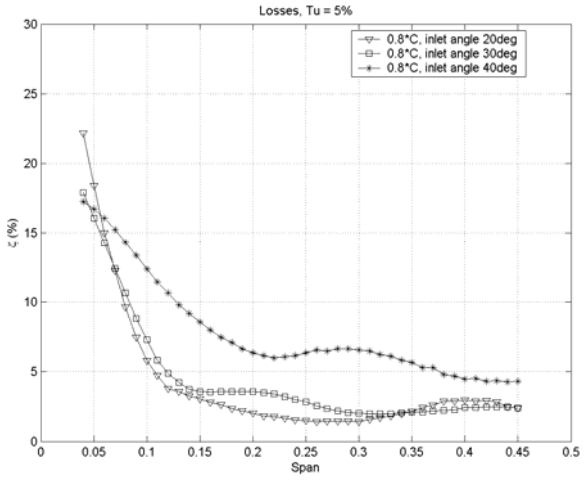

Figure 24 Losses for different inlet flow angles at the same downstream position 0.8*C and Tu=5%

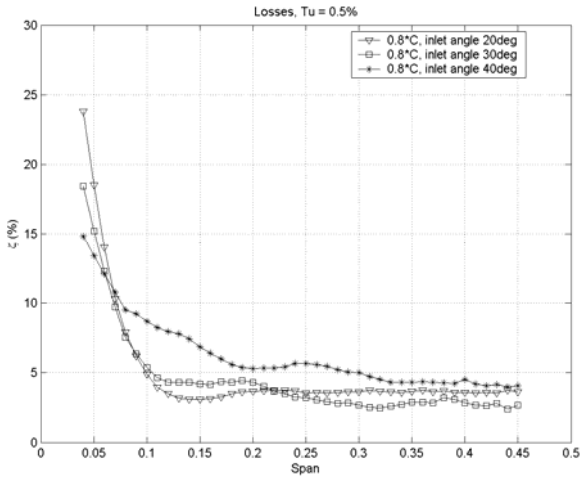

Figure 25 Losses for different inlet flow angles at the same downstream position 0.8*C and Tu=0.5%

5 CONCLUSIONS

This paper presents detailed experimental results for incidence and turbulence effects on three dimensional flows downstream of a LPT/OGV linear cascade. In addition to this the consequences of some boundary layer characteristics are also investigated. The results are summarized below.

- A good explanation of the downstream secondary flow field distribution can be developed from measurements of a 5-hole probe. The position, size and interactions of the main vortical structures are clearly visible and can be interpreted.
- The loading has an effect on the secondary flows intensity, relative position and absolute location.
- The turbulence intensity enhances the coherence of the vortical structures and their mutual interactions. Its limited influence on the mean flow field characteristics reduces as the turning increases.
- For the same overall vorticity content and shape factor, the thickness of the inlet boundary layer influences the secondary flows position and size. The vorticity concentration within the inlet boundary layer has an impact on the downstream vorticity magnitude.

As shown by Gregory-Smith and Cleak [2], the downstream flow field should now be investigated with cross wires in order to provide a more complete set of measurements to the modelers.

ACKNOWLEDGEMENTS

The present work is a part of the project COOL supported by the Swedish Gas Turbine Center (GTC), and funded by Siemens, Volvo Aero Corporation and Energimyndigheten. The permission for publication is gratefully acknowledged.

REFERENCES

[1] Sieverding, C. H., 1985 “Recent Progress in the Understanding of Basic Aspects of Secondary Flows in Turbine Blade Passages,” Transactions of the ASME, Vol. 107

[2] Gregory-Smith, D. G. and Cleak, J. G. E, 1992 ”Secondary Flow Measurements in a Turbine Cascade With High Inlet Turbulence,” Journal of Turbomachinery, Vol. 114

[3] Sharma, O. P. and Butler, T. L., 1987 ”Prediction of Endwall Losses and Secondary Flows in Axial Flow Turbine Cascades,” Journal of Turbomachinery, Vol. 109

[4]Wang, H. P., Olson, S. J., Goldstein, R. J. and Eckert, E.R.G., 1997 “Flow visualization in a Linear Turbine Cascade of High Performance Turbine Blades,” Journal of Turbomachinery, Vol. 119

[5] Goldstein, R. J. and Spores, R. A., 1988 “Turbulent Transport on the Endwall in the Region Between Adjacent Turbine Blades,” Transactions of the ASME, Vol. 110

[6] Kawai, T., Shinoki, S. and Adachi, T., 1990 “Visualization Study of Three-Dimensional Flows in a Turbine EndWall Region,” JSME International Journal, Series II, Vol. 33, No. 2

[7] Hjärne, J., Larsson, J. and Löfdahl, L., 2003, “Design of a Modern Test-Facility for LPT/OGV flows,” ASME Turbo Expo

[8] Hjärne, J., Larsson, J. and Löfdahl, L., 2005, “Experimental Evaluation of the Flow Field in a State of the Art Linear Cascade with Boundary-Layer Suction,” ASME Turbo Expo

[9] Arts, T., Boerrigter, H., Buchlin, J.-M., Carbonaro, M., Degrez, G., Dénos, R., Fletcher, D., Olivari, D., Riethmuller, M.L., Van den Braembussche, R.A., “Measurement Techniques in Fluid Mechanics”, 2nd revised edition, reprint of VKI LS 1994-01.

[10] Praisner, T.J., Smith, C.R., 2005, “The Dynamics of the Horseshoe Vortex and Associated Endwall Heat Transfer, Part I – Temporal Behavior”, ASME Turbo Expo.